AIAA 2001-2664

Application of OVERFLOW to Hypersonic Perfect Gas Flowfields

M. E. Olsen NASA Ames Research Center
Moffett Field, CA 94035

D. K. Prabhu Eloret Corp.
Sunnyvale , CA 94087

15th AIAA Fluid Dynamics Conference
June 11 - June 14, 2001 / Anaheim, CA

AIAA 2001-2664

Application of OVERFLOW to Hypersonic Perfect Gas Flowfields

M. E. Olsen *NASA Ames Research Center
Moffett Field, CA 94035

D. K. Prabhu †Eloret Corp.
Sunnyvale , CA 94087

A valiadation of the matrix dissipation option in OVERFLOW was completed, and a single set of constants was found which yield good inviscid shock capturing, viscous heat and skin friction predictions, and work over a wide Mach and Reynolds number range. This scheme works well with multigrid, and produces fast convergence to steady state for 2 and 3 dimensional problems, with accuracy comparable to Roe upwinding, and without 'carbuncle' problems for the blunt body flowfields.

Introduction

OVERFLOW[1,2] has been mainly applied to flow past subsonic, transonic and supersonic complex geometry vehicles. An investigation of the flow solver in the ideal gas regime is the first step in extending the capability of OVERFLOW to include non-equilibrium chemistry flowfields. The requirements for the flow solver were

- capable of handling strong shocks, yielding good post-shock conditions
- capable of providing a starting solution
- good skin friction and heat transfer predictions
- extensible to non-equilibrium chemistry flowfields

Matrix dissipation[3] mimics a TVD upwind biased scheme, within an underlying central spatial differencing framework. A commonly cited problem is the trial and error procedure needed to choose values for the smoothing parameters to ensure stability, and obtain solutions of high accuracy. A set of universal parameters has been found which will provide sufficient stability to converge inviscid blunt body flowfields, yielding correct shock strength for even moderately coarse grids. These parameters eliminate 'carbuncle' problems in these flowfields, and still provide accurate predictions of skin friction and heat transfer for flat plates for subsonic to supersonic flowfields. A further advantage is that these parameters, and the central/matrix dissipation scheme work well with the existing multigrid framework within OVERFLOW to rapidly converge to steady state. The scheme has been tested on moderate to high hypersonic Mach number flowfields, on 2D and 3D problems.

*Research Scientist, NASA Ames Research Center, Associate Fellow AIAA

†Senior Research Scientist, Eloret, Senior Member AIAA

Method

The scheme chosen here combines 2nd order central pacial differencing with the Swanson/Turkel matrix dissipation. When using this method, 4 adjustable parameters must be chosen: the coefficients of the 2nd and 4th smoothing(κ_2 and κ_4 in ref,[3] DIS2, and DIS4 in the OVERFLOW nomenclature), and two eigenvalue limiters(V_{ϵ_n}, V_{ϵ_n} in,[3] VEPSL and VEPSN for OVERFLOW). A single set of constants was found which satisfied the requirements enumerated above. Roe averaging was used to obtain the matrices used in the dissipation scheme since we are attempting to obtain a shock capturing scheme for high normal Mach numbers.

The constants used to obtain the results in this paper are:

$$\text{DIS2} = 2$$

$$\text{DIS4} = 0.1$$

$$V_{\epsilon_n} = 0.3$$

$$V_{\epsilon_l} = 0.3$$

The Pulliam-Chausee diagonal scheme, coupled with multigrid and grid sequencing is used for a relaxation scheme, providing fast and robust convergence.

Starting flowfields with detached shocks is the only time when the parameters of this scheme require adjustment. To obtain a starting solution, the flowfield is started from a uniform freestream on a very coarse grid (15 of every 16 points in the fine grid are dropped) with both eigenvalue limiters (V_{ϵ_l}, V_{ϵ_n}) set to unity. Setting the limiters to unity makes the dissipation mimic a scalar dissipation scheme. This produces a flowfield with a smeared, but correctly located shock, and does so very cheaply. The residuals should be dropped at least 3 orders of magnitude in this step. The solution thus obtained is quite amenable to allowing a shock fitted grid to be obtained with grid adaptation, if desired. The results of this paper were obtained without

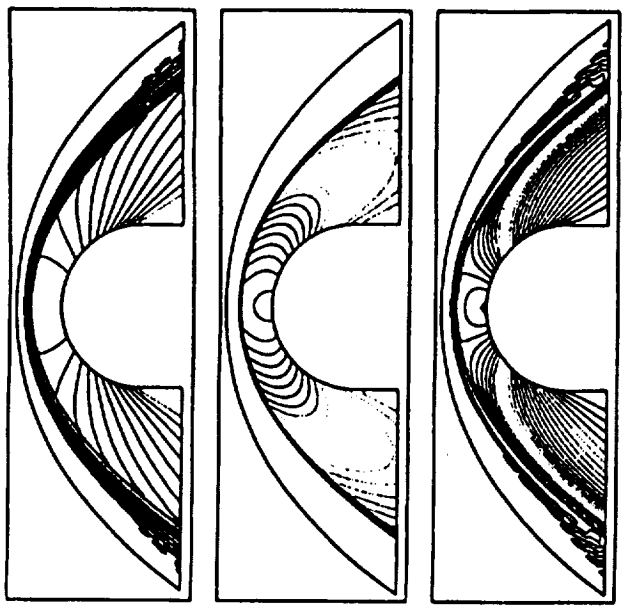

a) Pressure b) Temperature c) Density

Fig. 1 Inviscid $M_\infty = 32$ Blunt Body Flowfield

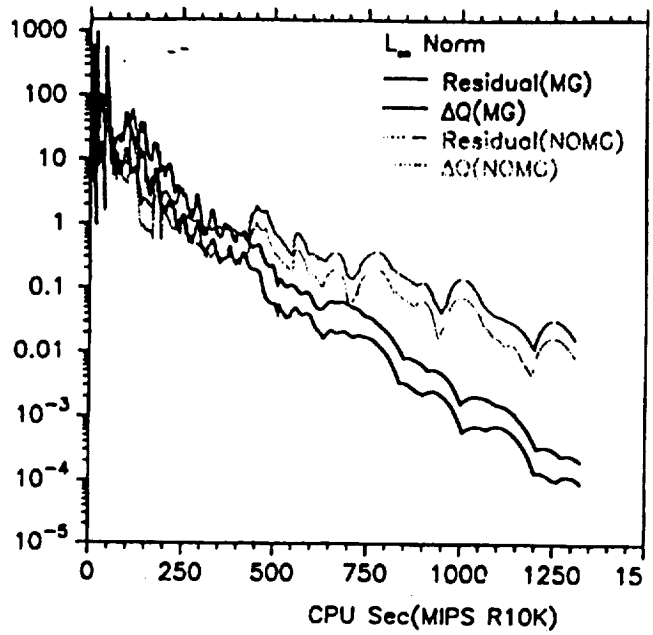

Fig. 2 Iteration History: $M_\infty = 32$ Blunt Body

a scalar dissipation scheme. This produces a flowfield with a smeared, but correctly located shock, and does so very cheaply. The residuals should be dropped at least 3 orders of magnitude in this step. The solution thus obtained is quite amenable to allowing a shock fitted grid to be obtained with grid adaptation, if desired. The results of this paper were obtained without any grid adaptation. After the starting solution is obtained, the solution is restarted with both V_ϵ parameters set to the recommended value of 0.3. Grid sequencing is recommended as well as multigrid.

Results

Inviscid Circular Cylinder

The overall flowfield is shown in Fig.1, with contours of the log of pressure.

This case is the inviscid flow past a blunt cylinder at various Mach numbers. This case was run at 3 Mach numbers: 8, 16 and 32, to obtain solutions with moderate to extreme shock pressure jumps. A 101 × 101 grid was the finest grid run, and cases with 51 × 51 and 26 × 26 are also shown, to exhibit the schemes ability to handle coarse grids robustly.

Convergence

The $M = 32$ case is considered as an example here, as it is the most challenging case to converge. An initial run to set up the starting solution was done as described above, with 600 iterations serving to lower the residual by 4 orders of magnitude.

Next the solution was restarted with the limiter parameters reset to the recommended values of $V_{\epsilon_n} = V_{\epsilon_l} = 0.3$, and through 3 stages of grid cycling which keep the "depth" of the multigrid method at 2. All these cycles were run using constant CFL of 0.8, and resulted in a fine grid residual reduction of 5 orders of magnitude for the first 1000 fine grid iterations. The residual histories are plotted in Fig.2 with residuals shown as a function of cpu seconds. The relative cheapness of the coarse grid cycles is graphically evident.

Fig.2 shows the ability of multigrid to accelerate convergence for this case. The residual history as a function of CPU seconds is shown for the fine grid solution with and without multigrid. Multigrid seems to provide faster and more robust convergence for the other flowfields we have investigated as well. That the multigrid scheme actually worked more reliably and at higher CFL numbers than non-multigrid for an inviscid flowfield with strong shocks was unexpected, but welcome. For viscous flowfields, the multigrid scheme greatly accelerates convergence.

Smoothing Parameters

The choice of smoothing parameters was fixed largely by this problem, with the "carbuncle problem" as the determining factor. When the 4th order smoothing value(DIS4) is lowered by a factor of two (from .1 to .05; Fig.3), or with the linear "limiter" set to $V_{\epsilon_l} < 0.3$, the temperature, density velocity and contours of this case begin to show signs of the carbuncle problem, where insufficient smoothing allows the solution to develop slope discontinuities in derivatives post shock in the stagnation region.

The 2nd order smoothing parameter, DIS2, can be increased from its recommended value. The only effects of increasing DIS2 are that the shock is smeared over more points, and the stagnation enthalpy(which should be constant for this problem) is less well conserved, as seen in Fig 4). For example, stagnation

the solution to develop slope discontinutities in derivatives post shock in the stagnation region.

The 2nd order smoothing parameter, DIS2, can be increased from its recommended value. The only effects of increasing DIS2 are that the shock is smeared over more points, and the stagnation enthalpy(which should be constant for this problem) is less well conserved, as seen in Fig 4). For example, stagnation enthalpy and stagnation pressures are altered by less than 1% if DIS2 is increased by a factor of 5. If DIS2 is decreased by a factor of 2, the scheme fails to converge.

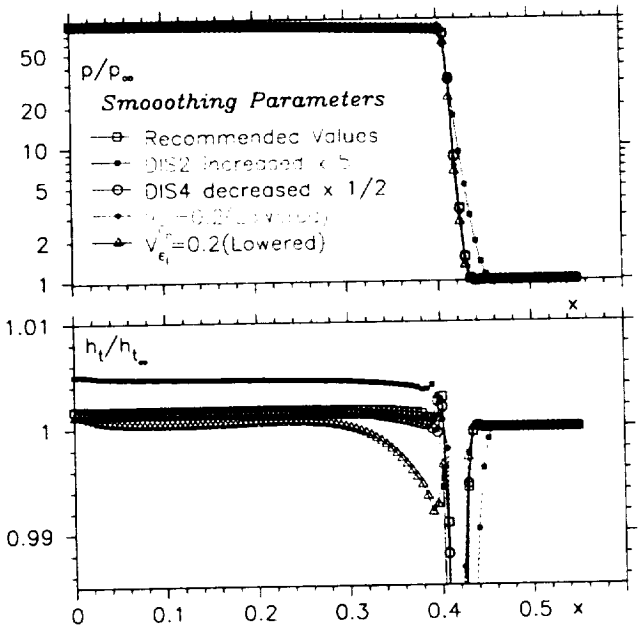

Fig. 4 Pressure and Stagnation Enthalpy Profiles Variations with Smoothing Parameter Choice, M = 8 case

A similar dependence on the nonlinear eigenvalue limiter $V_{\epsilon_n} < 0.3$ parameter is also shown. It is possible to decrease V_{ϵ_n} to 0.2, without creating slope discontinuities in the stagnation region, but convergence is not as rapid, with no obvious improvement in solution accuracy(Fig 4)). Increasing any of the smoothing parameters above their recommended values actually slows the convergence process. Although these results have been shown for the M = 8 case, these observations also hold true for the higher Mach numbers, at least up to M = 32.

Accuracy and Grid Requirements

In these discussions, the static pressure and stagnation enthalpy will be focused on, as these two variables will determine the wall boundary layer evolution for boundary layer flows. The accuracy to which these variables can be predicted directly affects the accuracy of the skin friction and heating predictions for viscous flows.

Stagnation line profiles of pressure and stagnation enthalpy for M = 32 case for solutions on coarse, medium and fine grids are shown in Fig 5. This case

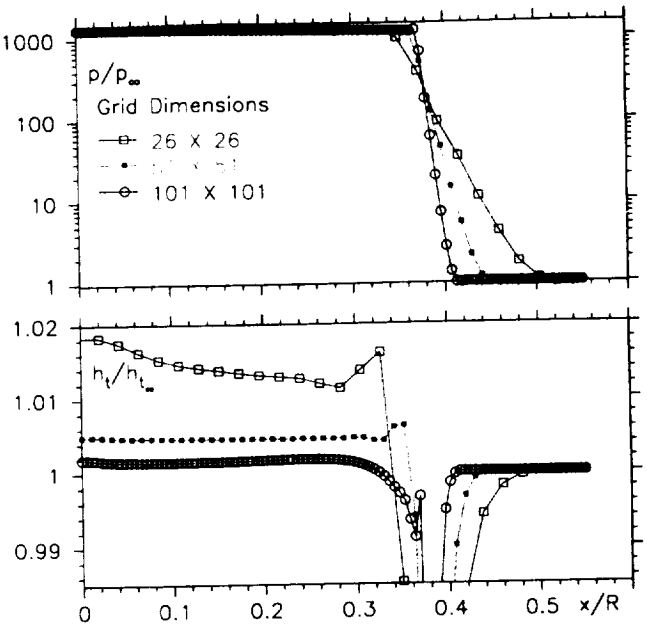

Fig. 5 M=32 Inviscid Blunt Body Stagnation Line Profiles For Various Grid Densities

has extremely strong shocks, with a shock pressure rise of 3 orders of magnitude. The stagnation point pressure is predicted to within 1% on all grids, with the finest grid within 0.1% of the theoretical value. Even on the coarse grids, the scheme produces good post-shock and stagnation predictions. The error in stagnation enthalpy is less than 2% on the finest grid at the stagnation point, and for the fine grid, the error is less than 0.2%. This ability to produce reasonable solutions on coarse grids is presumably the reason for matrix dissipation's good performance when coupled with multigrid.

It should be emphasized that all these solutions were obtained with the same values of DIS2, DIS4, V_{ϵ_n} and V_{ϵ_l}. The question now is whether with these smoothing parameters, viscous boundary layers can be accurately predicted. Thus, we are led to the flat plate test cases, where the ablity to accurately predict the boundary layer flow may be assessed.

Compressible Laminar Flat Plate

For this case, without a detached shock present in the flowfield, it is no longer necessary to obtain a starting solution (cycle 1 in the sequence outlined above). A single run of OVERFLOW is sufficient to obtain the solution for this case, and is made with the recommended parameters, with the full multigrid (grid sequencing) of 200 iterations on a coarse grid, 400 on a medium grid, and 400 iterations on the finest grid. Convergence was checked by running 1000 iterations further on the fine grid.

The laminar flat plate was run at M = 2, and M = 4, with adiabatic and constant temperature wall conditions, and a freestream temperature of 517.8°R. The grid for this case was 129 by 129. The skin friction

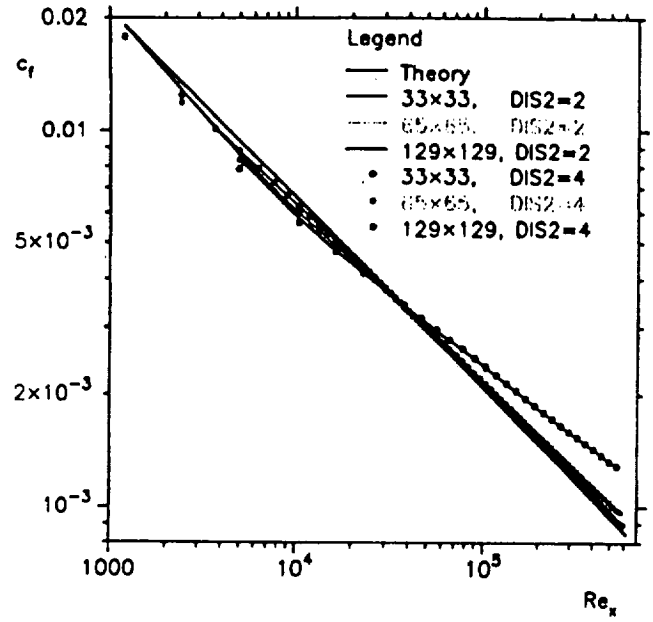

Fig. 6 Skin Friction, $M_\infty = 2$, $T_w = T_\infty$

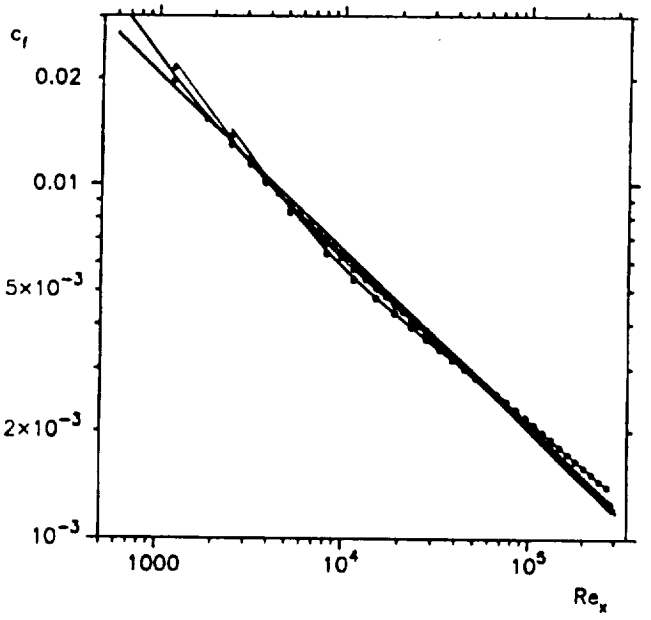

Fig. 7 Skin Friction, $M_\infty = 4$, $T_w = T_\infty$

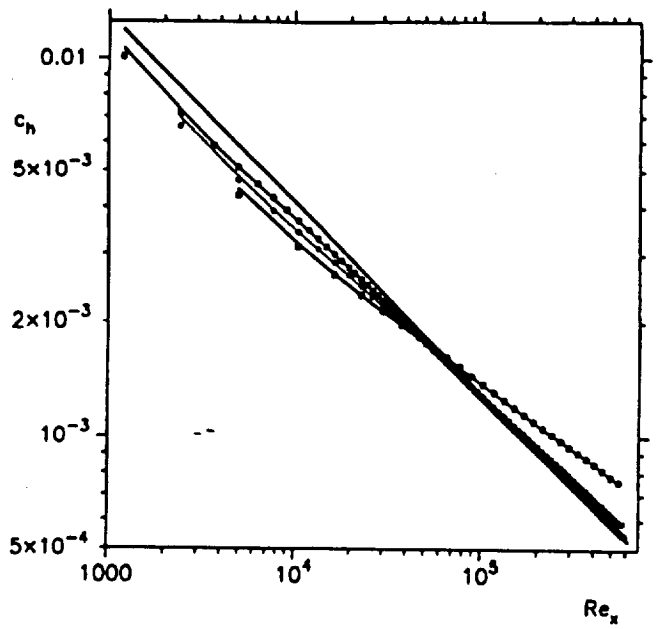

Fig. 8 Heat Transfer, $M_\infty = 2$, $T_w = T_\infty$

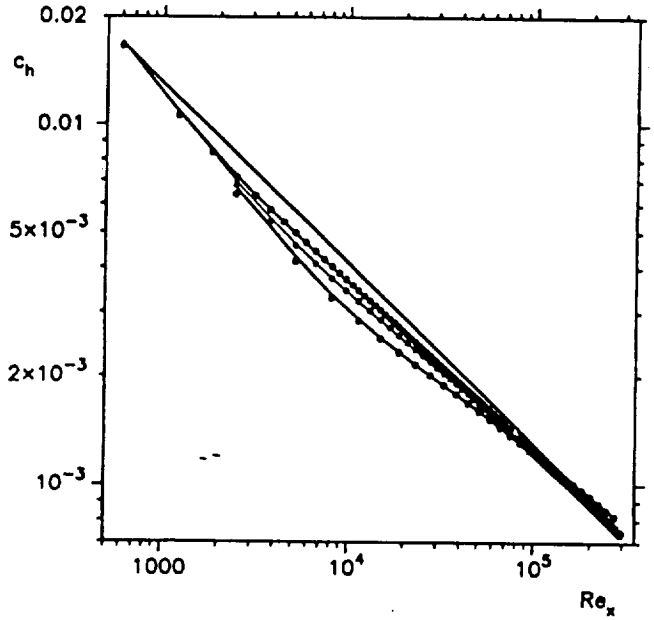

Fig. 9 Heat Transfer, $M_\infty = 4$, $T_w = T_\infty$

A single run of OVERFLOW is sufficient to obtain the solution for this case, and is made with the recommended parameters, with the full multigrid (grid sequencing) of 200 iterations on a coarse grid, 400 on a medium grid, and 400 iterations on the finest grid. Convergence was checked by running 1000 iterations further on the fine grid.

The laminar flat plate was run at $M = 2$, and $M = 4$, with adiabatic and constant temperature wall conditions, and a freestream temperature of 517.6°R. The grid for this case was 129 by 129. The skin friction comparisons for the $T_w = T_\infty$ cases are shown in Fig.6 and Fig.7. The wall heating rate (c_h) comparisons are shown in Fig.8 and Fig.9. The heating rate predictions and skin friction are in very good agreement with theory over the entire plate. These figures also demonstrate the independence of these predictions to variations in the 2nd order smoothing coefficient, as the plots show open symbols with the recommended smoothing values, and filled symbols solution results with DIS2 increased by a factor of 2.

Now, the inviscid shock capturing ability and the ability to model viscous flows has been demonstrated in isolated cases. We are now led to a simple case involving both shocks and viscous effects, the viscous circular cylinder.

Viscous Circular Cylinder

Given this good agreement for the inviscid blunt body and viscous flat plate, a natural question is how

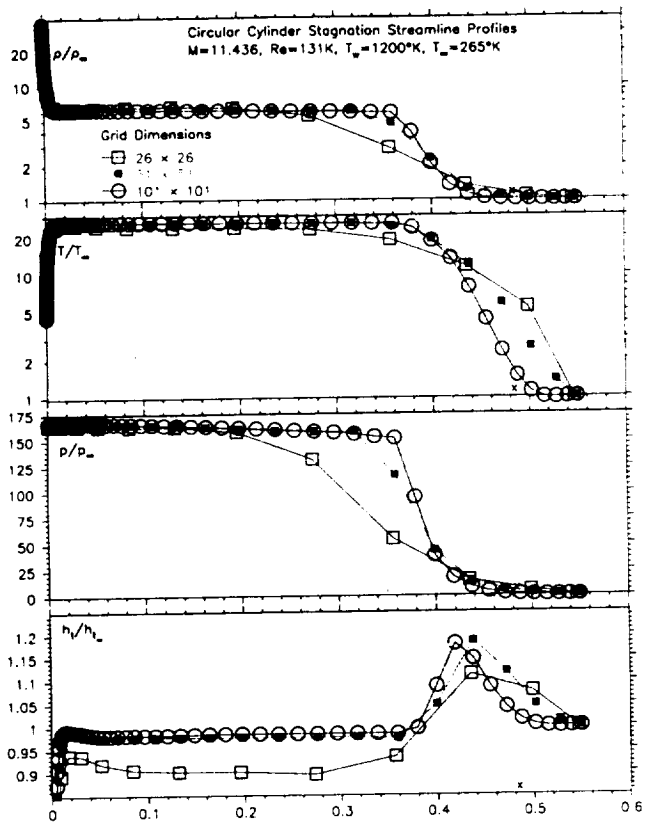

Fig. 10 Stagnation Line Profiles for Viscous Circular Cylinder, $M_\infty = 11.436, T_w = 1200.°K, T_\infty = 265°K$

51 × 51 grid was obtained from the original grid by removing every other point from the finer grid, and the 26 × 26 grid was obtained similarly from the 51 × 51 grid.

The stagnation line profiles for this case are shown in Fig.10. The adiabatic wall temperature for this case is 6146.53°K, so that if the freestream enthalpy is 1% low downstream of the shock, the heat transfer predictions would be expected to be 1.3% low. The fine and medium grids have an enthalpy about 2% low, and the coarse grid has an total enthalpy 10% low. All grids predict the same pressure profile, but the post shock temperature is lower and the density higher on the coarse grid, consistent with the low total enthalpy post shock.

The stagnation point heating rates are predicted reasonably well on all grids (Fig.11), with the fine grid 1.% low, the medium grid 1.1% high and the coarse grid 10% high. The overprediction of heat transfer on the medium and coarse grids is due to the coarser wall resolutions and the slight overshoots in total enthalpy at the boundary layer edge.

The fine grid in this case required a higher 2nd order smoothing (DIS2=4, twice the "recommended" value) in order to achieve convergence in c_h. The heating rate prediction was far more sensitive to solution convergence than quantities like pressure were. Small variations in the solution which could not be

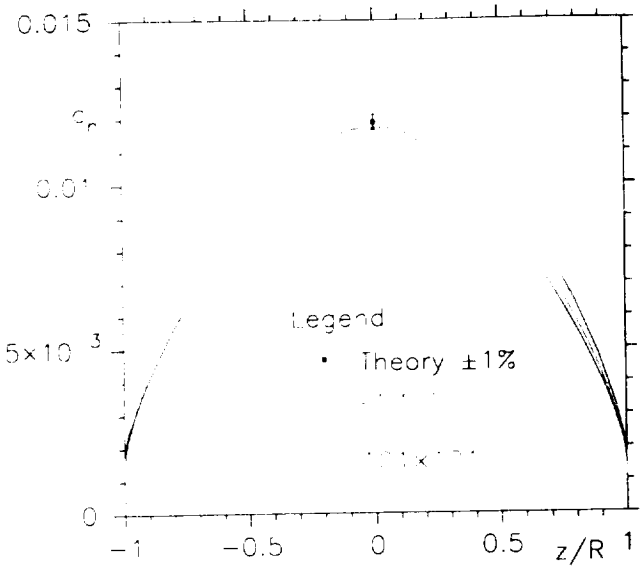

Fig. 11 Heating Rate Predictions, for Viscous Circular Cylinder, $M_\infty = 11.436, T_w = 1200.°K, T_\infty = 265°K$

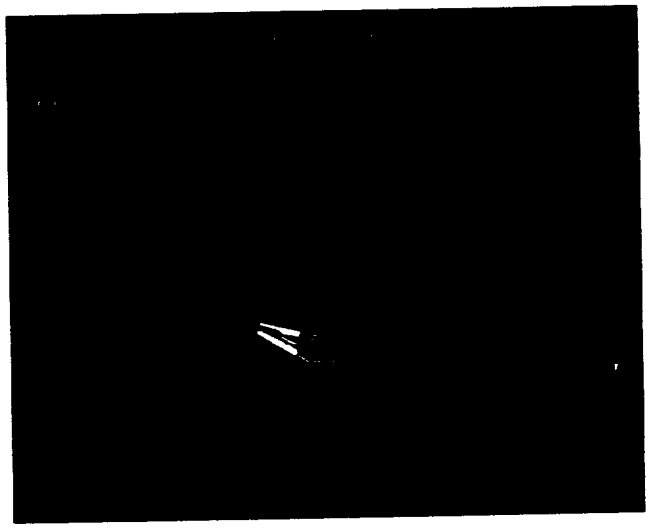

Fig. 12 Cylinder Flare Flowfield, $M_\infty = 9.91, T_w = 293°K, T_\infty = 51°K$

discerned to plotting accuracy in the stagnation line profiles could make large variations in the heat transfer coefficient.

Now, the ability to handle attached viscous flows with shocks has been demonstrated. The next element of flow complexity to be checked is the ability to model high speed separated flows.

Viscous Cylinder-Flare

This case[4,5] is a hollow, finite length cylinder, with a 10° flare. The flowfield exhibits a laminar separation bubble. This flowfield requires a large number of iterations to converge as the laminar separation slowly creeps upstream. Fig.12 shows the geometry along with the pressure field contours for a converged 321 × 301 grid solution.

A grid convergence study was completed for this

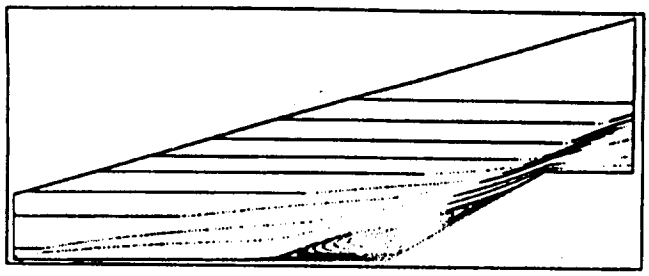

Fig. 12 Cylinder Flare Flowfield, $M_\infty = 9.91, T_w = 293°K, T_\infty = 51°K, p_\infty = 52Pa$

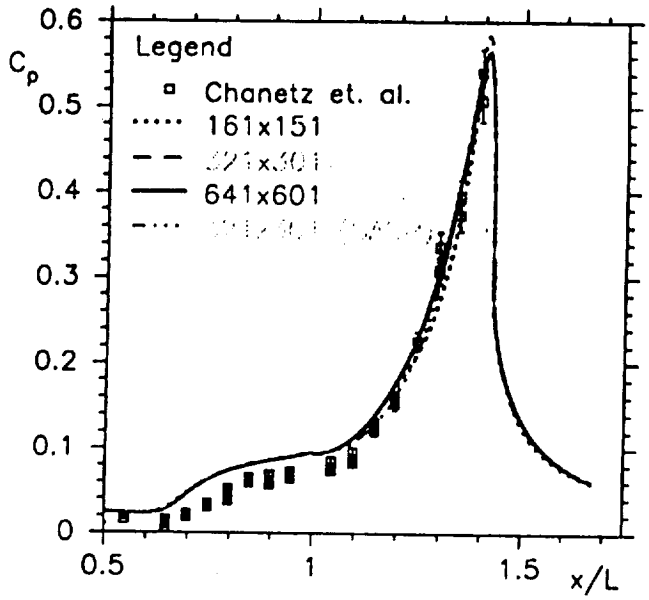

Fig. 13 Cylinder Flare Surface Pressure

most clearly shown in Fig.14, which also shows a similar grid convergence. The heat transfer predictions are similarly grid converged(Fig.15).

As noted previously, this flowfield required many iterations to converge, with the laminar separation moving slowly up the cylinder in the subsonic portion of the boundary layer. Over 10,000 iterations for the 321 × 301 grid, and 6,000 iterations for the 161 × 151 grid were required to reach the steady state solution. The solutions were run out (to 40,000 iterations for the 321 × 301 solution) to confirm the convergence of the relaxation process. Sage[7] was used to obtain the 621×601 grid, which also gave a very respectable starting solution. This solution was run out an additional 10,000 iterations to confirm its relaxation convergence.

The pressures predicted by both codes are above the experimental data upstream of the flare, similar to the experimental/computational comparisons by Chanetz.[5] The pressures predicted on the flare are in good agreement with the data, as well as each other. The separation location predicted by both codes (X/L=0.7) is slightly upstream of the reported experimental value($X/L = 0.76 \pm 0.01$), but the reattachment point (X/L=1.35) agrees with the experimental value ($X/L = 1.34 \pm 0.015$). The heat transfer

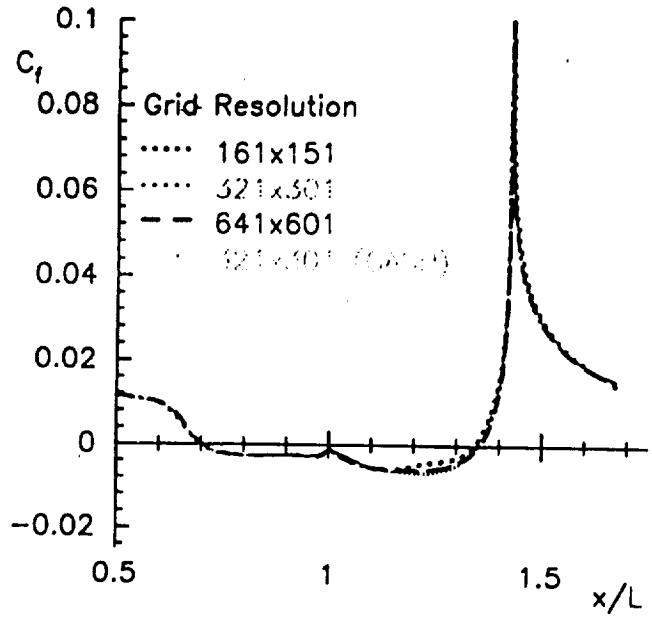

Fig. 14 Cylinder Flare Skin Friction

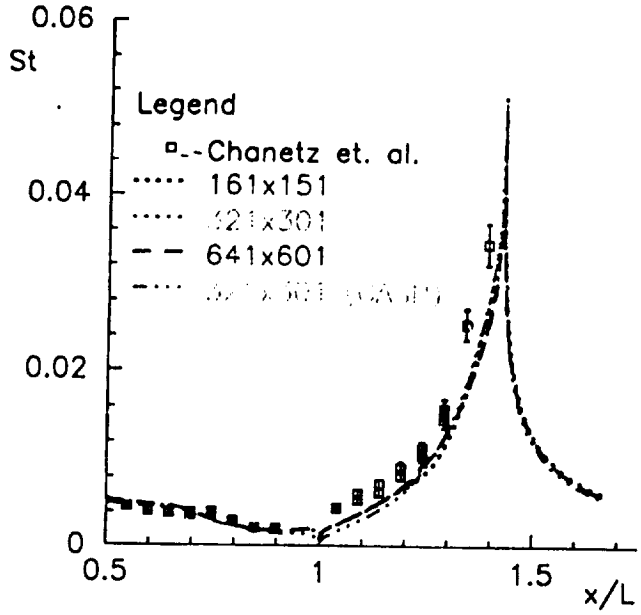

Fig. 15 Cylinder Flare Heat Transfer

predictions are in good agreement with each other, and experiment.

With the ability to handle this level of flow complexity in two dimensions, the next logical step is 3 dimensional flowfields.

3D Flowfields

The scheme described here has been successfully applied to X38 forebody, "Sharp", Shuttle and X33 grid systems. Here we will focus on the solution about the X33 geometry, as this used the complex geometry (chimera) capabilities of OVERFLOW.

The starting point for this grid system was the patched grid used to solve the flowfield with GASP. Preliminary computations utilized a chimera grid system obtained by simply extending the patched system

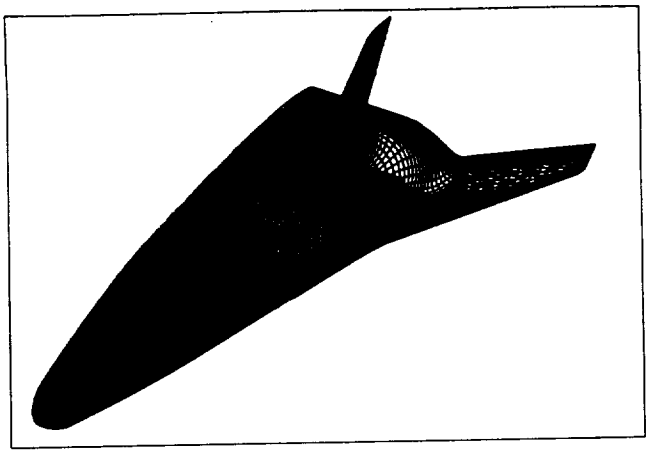

Fig. 16 X33 Surface Grid System

patched grid used to solve the flowfield with GASP. Preliminary computations utilized a chimera grid system obtained by simply extending the patched system grids into each other to provide sufficient overlap for the chimera scheme to work.

Solutions obtained on this grid system appeared adequate, with pressure and heat transfer plausible over the vehicle surface. There was, however an underlying problem, in that the chimera overlap surface included the stagnation point flow. With the minimal overlap created with this grid system, the surface pressure predictions were very good, but the heat transfer predictions, even when the grid appeared to be fully converged, were off by a factor of two.

A new nose grid fully enclosing the stagnation point was rapidly generated using the chimera grid tools package (Fig.16) and the solution was re-run. The pressure predictions obtained agreed with those obtained on the first grid system, and the heat transfer predictions came into line with those expected from previous GASP solutions,[8] and experiment.[9-11]

This solution required a residual reduction of 8 orders of magnitude in order to provide good heat transfer estimates. Multigrid was again quite useful, although it had to be shut off in the aft grid which contains the wings and winglets. The upstream chimera join (near the nose) is a true chimera interface, where there are no coincident points. The downstream interface was created simply to break the body grid into two zones, in order to facilitate the parallelism of the solution process. This interface has coincident surfaces.

The surface flow patterns are continuous across the chimera zone boundaries along the surface, as can be seen in Fig.19. Furthermore, the zonal boundaries intersect the bow shock on all three grids (Fig.20). On both of these boundaries, the chimera system provides sufficient solution continuity even for heat transfer estimates.

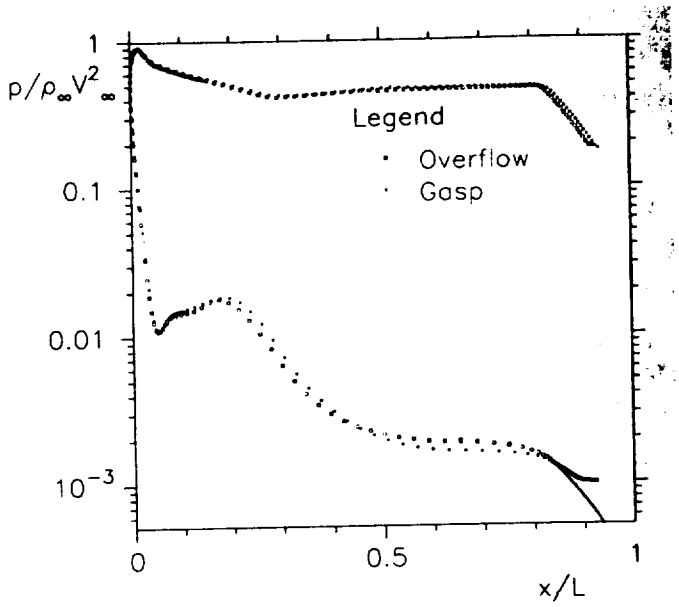

Fig. 17 X33 Centerline Surface Pressures, M_∞ = 5.98, $\alpha = 40°$, $Re_L = 3.3 \times 10^6$

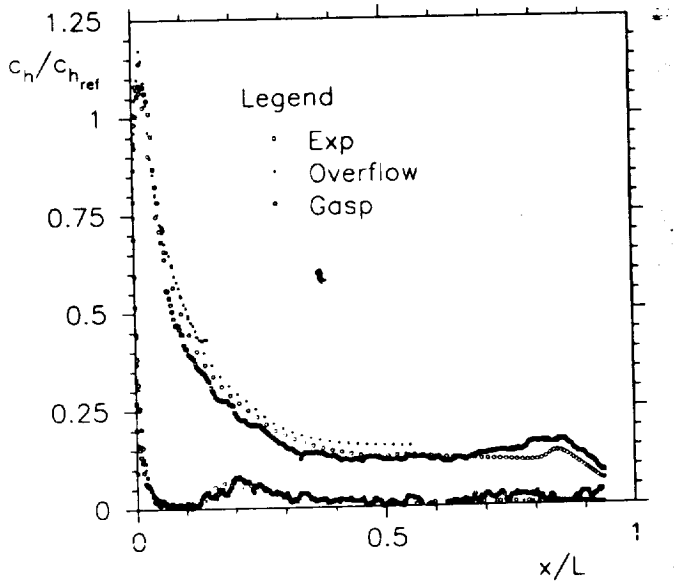

Fig. 18 X33 Centerline Heat Transfer, $M_\infty = 5.98$, $\alpha = 40°$, $Re_L = 3.3 \times 10^6$

Discussion

This work extends a number of innovative extensions of subsonic technology into the high speed world. Matrix dissipation has been used successfully in transonic flowfields, and can yield predictions which are of the same quality as upwind MUSCL schemes, at much lower computational cost. This was found to be true even at high Mach numbers, with M = 32 normal shocks nicely modelled, even on coarse grid systems. Furthermore, one set of constants was found which can reliably used on all the grid systems tested here. While some attention was paid to keeping grid stretching below 1.2, and reasonably orthogonal grids, the grids used were generated with standard grid gen-

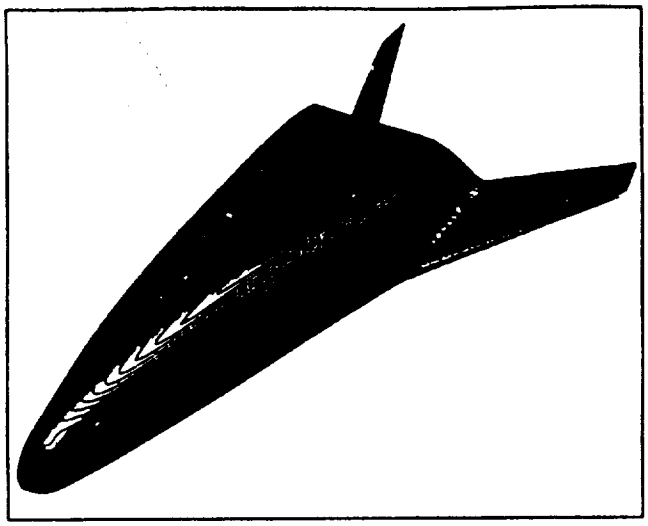

Fig. 19 X33 Surface Pressure Contours, $M_\infty = 5.98$, $\alpha = 40°$, $Re_L = 3.3 \times 10^6$

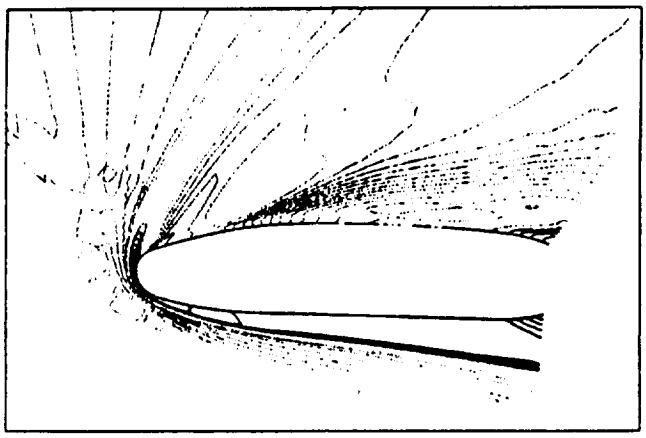

Fig. 20 X33 Symmetry Plane Pressure Contours, $M_\infty = 5.98$, $\alpha = 40°$, $Re_L = 3.3 \times 10^6$

high speed flows to speed time to solution. Multigrid as part of the solution process does not seem to be as widespread, especially in the structured grid world. Multigrid was found to be valuable in speeding up the convergence process, on both Euler and viscous grid systems. For solutions where extremely large residual reductions are required, such as heating rate prediction cases, this is invaluable.

Another piece of transonic technology which worked well at hypersonic speeds was the Pulliam-Chausee diagonal algorithm. Although coupling this solution algorithm with chemistry is problematic, for solutions where the mean flow and chemistry systems can be solved in an uncoupled manner, this algorithm promises large computational cost savings.

The solution of the X33 system shows the feasibility of using the chimera system for high speed flowfields. The ability to use chimera to model complex geometries greatly facilitates the ability to obtain predictions for flight vehicles, and allows the tailoring of grid systems component by component. For rapid evaluation of an evolving system design, this capability is extremely important.

Conclusions

Matrix dissipation combined with multigrid and grid sequencing shows promise as a method to solve hypersonic Mach number flowfields. The solutions obtained are as accurate as upwinding schemes, and appear to converge more quickly, especially when combined with multigrid. The chimera methodology also shows promise in this regard. In addition to providing a simple means to model flows about complex geometries, the solutions obtained can be made sufficiently continuous across zonal boundaries.

This work is part of a overall effort to use OVERFLOW to predict vehicle re-entry flowfields. The scheme provides a fast, robust, and accurate means of solving the Navier-Stokes equations at hypersonic Mach numbers.

References

[1]Buning, Pieter. G et al. Overflow user's manual. Version 1.8, NASA Ames Research Center, February 1998.

[2]Jespersen, D, Pulliam, T. H., and P.G. Buning. Recent enhancements to overflow. AIAA Paper 97-0664, January 1997.

[3]Swanson, R. C. and Eli Turkel. "On Central-Difference and Upwind Schemes". *Journal of Computational Physics*, 101:292-306, 1992.

[4]Chanetz, B., Benay, R. J., Bousquet, J.M, Bur, R., Oswald, J., Pot, T., Grasso, F., and Moss J. "Study of the laminar shock wave/boundary layer interaction in hypersonic flow: experimental and numerical aspects". ONERA TP 1997-182, 1st Europe-US High Speed Flow Field - Database workshop, , November 12-14 1997, Naples Italy, 1997.

[5]Chanetz, B., Bur, R., Pot, T., Pigache, D., Grasso, F., and Moss J. "Experimental and numerical study of the laminar separation in hypersonic flow.". ONERA TP 2000-212, ECCOMAS 2000 - European congress on computational methods in applied sciences and engineering, September 11-14 2000, Barcelona Spain, 2000.

[6]"GASPex Version 3 Users Manual". AeroSoft, Inc., 1872 Pratt Drive, Suite 1275, Blacksburg, VA 24060-6363, 1997.

[7]Davies, C. B. and E Venkatapathy. "The Self-Adaptive Grid codE:SAGE, Version 3". NASA TM 1999-208792, August 1999.

[8]Prabhu, Dinesh K., Wright, Michael J., Marvin, Joseph G., Brown, James L., and Ethiraj Venkatapathy. "X-33 Aerothermal Design Environment Predictions: Verifiation and Validation". AIAA Paper 2000-2686, 34th AIAA Thermophysics Conference , June 19-22 2000, Denver CO, 2000.

[9]Merski, N. R. "Reduction and Analysis of Phosphor Thermography Data with the IHEAT Software Package". AIAA Paper 98-0712, 1998.

[10]Merski, N. R. "Global Aeroheating Wind-Tunnel Measurements Using Improved Two-Color Phosphor Thermography Method". AIAA Paper 98-0712, 1998.

[11]Hollis, B. R., Horvath, T. J., Berry, S.A, Hamilton, H.H., and S.J. Halter. "X-33 Computational Aeroheating Predictions and Comparisons with Experimental Data ". AIAA Paper 2000-2686, 34th AIAA Thermophysics Conference , June 19-22 2000, Denver CO, 2000.

[10]Merski, N. R. "Global Aeroheating Wind-Tunnel Measurements Using Improved Two-Color Phosphor Thermography Method". AIAA Paper 98-0712, 1998.

[11]Hollis, B. R., Horvath, T. J., Berry, S.A, Hamilton, H.H., and S.J. Halter. "X-33 Computational Aeroheating Predictions and Comparisons with Experimental Data ". AIAA Paper 2000-2686, 34th AIAA Thermophysics Conference , June 19–22 2000, Denver CO, 2000.